IAC-03-U.2.b.02

LINEAR TWO-AXIS MOEMS SUN SENSOR AND THE NEED FOR MEMS IN SPACE

Martin Pedersen*, Jan H. Hales*, and René W. Fléron
(s991237@student.dtu.dk, s973712@student.dtu.dk, rwf@mic.dtu.dk)

Mikroelektronik Centret (MIC)
Technical University of Denmark (DTU)
DK-2800 Kgs. Lyngby, Denmark

ABSTRACT

The main topic of this paper is the linear two-axis Micro Opto Electro Mechanical System (MOEMS) sun sensor developed for the pico satellite DTUsat; the size of the sensor chip is $\sim 7 \times 8\text{mm}^2$. The sensor has a Field of View (FOV) of $\pm 70°$ and a resolution better than $1°$ is obtainable for $-40°$ to $40°$; beyond these angles resolution below $1°$ is difficult. One complete sensor chip along with needed measurement and interface electronics has been implemented on a $3.9 \times 5\text{cm}^2$ PCB with a mass of 7.1g.

In the paper an overview is first given of DTUsat followed by descriptions of functionality, design, realisation, integration, and performance of the sun sensor.

Furthermore the paper includes a discussion on the topic Micro Electro Mechanical Systems (MEMS) in space since it is the authors' opinion that the space society is missing out on many of the advantages MEMS can bring. MEMS can improve many traditional systems and enable construction of devices not possible with traditional techniques. On DTUsat MEMS had to be employed to contain the desired complexity in the CubeSat frame.

*M.Sc. student at Mikroelektronik Centret (MIC).

Copyright Statement Stamp

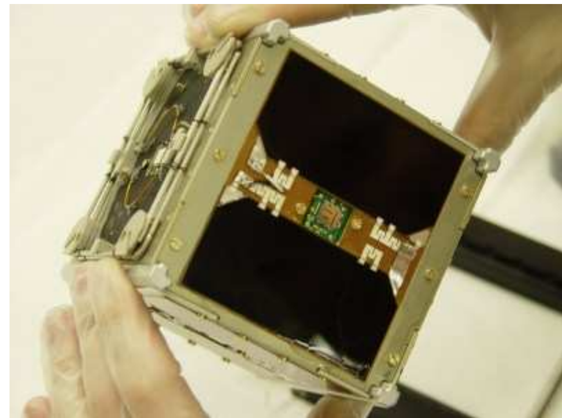

Figure 1: DTUsat in the assembly phase.

1 THE DTUsat PROJECT

In the summer of 2001 a group of students at the Technical University of Denmark (DTU) teamed up with the idea of building and launching a satellite in just one year! This very ambitious goal – none of the students had experience with satellite construction – was made to keep the motivation going during the entire project phase. It was thought that the students would be less interested if their project would not be launched while they were still students. However, after the initial design phase the suggested satellite was too complex to be realised in just one year. Instead of making a simple and "boring" satellite it was decided to extend the project to two years – the DTUsat project was born.[†] This also proved wise since finding a launch provider for a CubeSat[6] ended up being a very difficult task which was only

[†]More info on DTUsat can be found on its web page at http://www.dtusat.dtu.dk/.

accomplished due the great assistance provided by the Danish Space Research Institute (DSRI).

A group of ∼ 70 students have been involved with the project and ∼ 15 students have been fully involved during the entire project.

The CubeSat concept was chosen since it allows launch costs of only 35,000-70,000USD per satellite. The CubeSat gives all the basic mechanical constraints; e.g. it must be $10 \times 10 \times 10\text{cm}^3$ and have a mass of max 1kg.

DTUsat, which can be seen in figure 1, is divided into six different sub systems. These are briefly described in the following.

Power utilises solar panels on four sides and is capable of delivering ∼ 1.5W. The battery provides additional power during radio transmission where the power consumption exceeds the available solar energy. Latch-up protection is also included in this sub system.

On-Board Computer (OBC) contains of course CPU, ROM, RAM, Flash-RAM etc. Furthermore OBC serves as a motherboard on DTUsat since all PCBs (except sun sensors and camera) are mounted on the OBC.

Radio communicates in agreement with AMSAT with the ground station at 437.475MHz. The antenna is circular polarised and sufficiently omnidirectional to operate without attitude control.

ACDS contains a 4-axis magnetometer, two-axis sun sensors on five of DTUsat's sides, and three 1μNm PWM magnetotorquers mounted on the inside of three side panels. A close-up of the sun sensor is shown in figure 2.

Tether Payload is the scientific mission. After 1-2 months a 500m electrodynamic tether will be deployed to demonstrate lowering of the orbit due to interaction with the geomagnetic field. It was intended to increase the speed of the altitude change by emitting electrons with a MEMS emitter.[1] However this is not possible since the emitter was not finished in time.

Camera Payload is the public relations payload. Its original purpose was to produce pictures of Denmark, but since the camera electronics was not finished in time only a one pixel infrared camera is present. This can be used to investigate the temperatures the CCD will be exposed to with the developed lens.

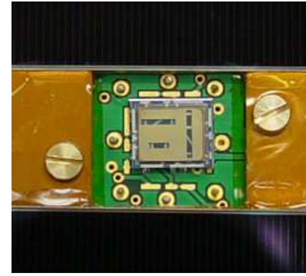

Figure 2: Close-up on a sun sensor.

DTUsat was launched on June 30 at 14:15:12GMT from Plesetsk, Russia. However this far contact has not been established. DTUsat was in the same P-POD as the other Danish student satellite AUC CubeSat and the Canadian Can-X with whom only AUC CubeSat has been able to establish radio contact. Investigation of why contact has not been established is currently being conducted. However, it can to some extent be caused by its complexity which only left very short time for testing while AUC CubeSat is more simple and had more time for testing.

Naturally it is disappointing that contact has not been established, but seen in the light of the fact that it is build by students on a low budget just finalising the satellite was a huge milestone in itself. It is the current intention to launch a $\text{DTUsat}X\big|_{X=1,2,3\ldots}$ every second year since the project produces *real* engineers; that is the students must combine many professions with practical applications. Hopefully the next DTUsat will be a success since it will not be build from scratch.

2 SENSOR PRINCIPLE

The sun sensor device presented in this paper is an analog slit sensor with triangular photodiodes. Figure 3 depicts the general design of one axis. As depicted the chip is realised with a Silicon On Insulator (SOI) – Pyrex sandwich structure. The Pyrex (borosilicate glass) part acts as a lid where sun rays only enter through the slit, and the SOI wafer contains the needed photodiodes. The difference between the generated photo currents in the triangular diodes is used to find the angle of the incoming sun rays, and the current from the rectangular reference cell is used to eliminate unwanted parameters.

By placing two one-axis sensors perpendicular to each other – as seen in the chip layout in figure 6 – a two-axis sensor is realised. The sensor chips flying

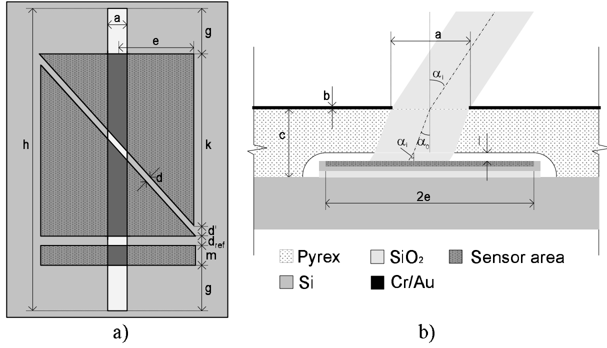

Figure 3: Sketch of the sun sensor (one axis). a) top view, b) cross sectional view.

on DTUsat are $7 \times 8\text{mm}^2$ and weighs 116mg.

A SOI wafer is used since it enables complete electrical insulation by etching away the top monocrystalline Si-layer. These grooves are created between all diodes and is continued all the way through the oxide layer to the bulk-Si to allow anodic bonding of the sandwich structure.

The cosine factor of the ideal photo current is given by $\cos(\alpha_k)\cos(\alpha_e)$ where α_x are the sun rays' angles about the k and e axes. By selecting the length g large enough the illuminated area is made independent of the α_e angle.

DTUsat is a CubeSat and hence cubic[6], which means that complete coverage can be obtained by designing for ±FOV larger than $\arctan(\sqrt{2a^2}/a) \approx 55°$ and placing one two-axis sensor on each side. This was an initial requirement[2]; however later for structural reasons it was decided to omit sun sensors on the payload side. The final FOV is well above the initial requirement.

The reference area can furthermore be used as a temperature sensor. An angle measurement allows calculation of the sun power exposed to the sensor since the sun power is relatively constant over time. By using this the temperature can be determined by knowing the sensors temperature dependence, which can be found to good precision both analytically and from measured characteristics.

2.1 Unwanted Parameters

The reference area in figure 3 can be used to cancel out several unwanted parameters. This is done by dividing the difference signal with the reference signal, and utilising that constant physical properties over the mono-Si layer can be assumed; however minor errors may be present due to surface recombination at the insulation grooves. The reference area has constant illuminated area:

$$A_{ref} = (a - s)m\Big|_{s=b\tan(\alpha_{ki})} \approx am \qquad (1)$$

since the shadow effect s of the slit can be neglected due to the low height b of the deposited metal (nm regime). If the difference between the generated triangular diode currents currents is used to find α_k then the result for the ideal case is ($\frac{P}{A}$ sun power per square metre, $A_t(\alpha_k)$ illuminated area of one triangle, $V(T)$ diode forward voltage, and η the efficiency):

$$\begin{aligned}\frac{\Delta I}{I_{ref}} &= \frac{I_{t2} - I_{t1}}{I_{ref}} \\ &= \frac{\frac{\frac{P}{A}\cos(\alpha_a)\cos(\alpha_b)}{V(T)}\eta\left(A_{t2}(\alpha_k) - A_{t1}(\alpha_k)\right)}{\frac{\frac{P}{A}A_{ref}\cos(\alpha_a)\cos(\alpha_b)}{V(T)}\eta} \\ &= \frac{A_{t2}(\alpha_k) - A_{t1}(\alpha_k)}{A_{ref}} \qquad (2)\end{aligned}$$

From this it is seen that the sensor can be made independent of the cosines and the temperature in $V(T)$ (the most significant T dependence of solar cells). Cancelation of $V(T)$ also removes most dark current effects, and cancelation of η removes dependence of sensor degradation due to radiation. Elimination of $\frac{P}{A}$ cancels disturbances caused by sun power fluctuations, and the albedo intensity contribution.

The angular disturbance from albedo is minimised by having maximum sensitivity in the short wavelength regime. More info on this can be found in section 4.

Note that the transmission term $(1 - R(\alpha_k))$ – which has no characteristic effect – has been left out in the second line of (2) for formatting reasons

When the method illustrated in (2) is used the output signal is only a function of the illuminated areas in the ideal case.

3 SENSOR DESIGN

Equation (2) in the ideal case for increasing illuminated area $A_{t1}(\alpha_k)$ and decreasing $A_{t2}(\alpha_k)$ can be found by using the geometry in figure 3:

$$\frac{\Delta I}{I_{ref}} = \frac{(-2(c-l)\tan\alpha_{ko} - 2l\tan\alpha_{ki} - s)k}{2em} \quad (3)$$

$$\alpha_{ko} = \arcsin\left(\frac{n_1}{n_2}\sin(\alpha_{ki})\right)$$

where $s = b\tan\alpha_i$ is the shadow effect from the slit. n_1/n_2 are the refractional indices for vacuum/Pyrex.

Dimensions of a, e, k, and l are important for the final characteristics of the device. The sensor is dimensioned from a desired current of 100μA at $\alpha_k = 0°$:

$$I_{t,0°} = \frac{\frac{P}{A}\frac{1}{2}ak}{V(T)}\eta(1-R(\alpha_k)) \Leftrightarrow$$

$$k = \frac{2I_{t,0°}V(T)}{a\frac{P}{A}\eta(1-R(\alpha_k))} \quad (4)$$

Large value of k ($\Rightarrow$ narrow slit length a) is desired for large changes in $A_t(\alpha_k)$, but contrarily wide a is needed for a small reference cell height m. m is also selected from the desired current at $\alpha_k = 0°$. e is given from the selected FOV.

Common for all measures is that they should cause relatively large $\frac{dI}{d\alpha_k}$ for most α_k to ensure high sensitivity.

Non-linearity is introduced with $\tan(\alpha_i)$ since $\alpha_i \geq \alpha_o$ in equation (3); see figure 4. Therefore l should be selected as low as possible; however, since the Pyrex and SOI wafer are anodically bonded l should still be large enough to avoid bonding to the active sensor areas – and hence destruction of the pn junction. That the latter problem only plays a role for very small l can easily be verified.[7]

Even though the reflection is canceled out in (2) and (3) it should be noted that this is important for the actual amplitudes of generated photo currents. The total reflection in the vacuum-Pyrex and the Pyrex-cavity transition of both the transverse electric and magnetic (TE/TM) polarised light waves can easily be deducted from the Fresnel equations.[‡] This yields the results shown in figure 5. From this it is seen that the desired FOV = 70° is obtainable since the total reflection still is relatively low at this point – < 25%. At the same time the figure shows that aiming for a much higher FOV is pointless since the reflection increases rapidly after 70°.

[‡] It is assumed that the reflected light in the Pyrex-cavity transition will not be reflected back in the vacuum-Pyrex transition.

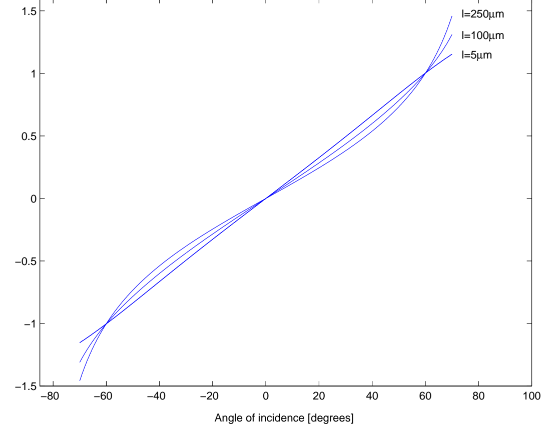

Figure 4: $\frac{\Delta I_t}{I_{ref}}$ graphs. The Pyrex-sensor distance l influences the linearity.

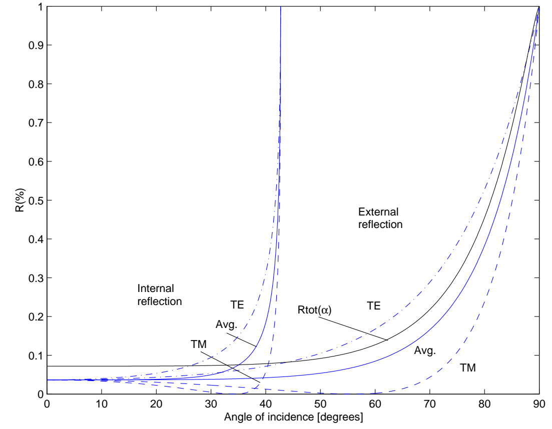

Figure 5: Reflectance in the vacuum-Pyrex transition (external), in the Pyrex-cavity transition (internal), and the total reflection.

Figure 6 illustrates the dimensions chosen for the sensor. A very conservative design was selected because short development time and first time success was needed. Although it is not necessary each signal from the chip is feed individually out to keep the chip design as versatile as possible.

Figure 7 shows plots of the ideal currents characteristics for the chosen geometry. In figure 4 the graph of $\Delta I_t/I_{ref}$ for $l = 5\mu$m shows the ideal output with the chosen geometry and measurement principle.

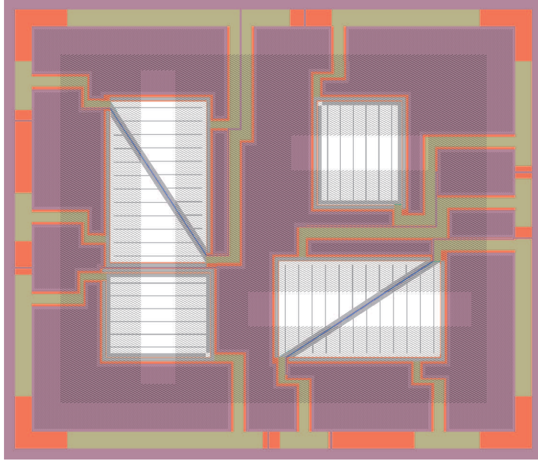

Figure 6: The seven masks for the sensor superimposed on top of each other. Chip size $\sim 7 \times 8\text{mm}^2$. One wafer stack contains approximately 100 sun sensors.

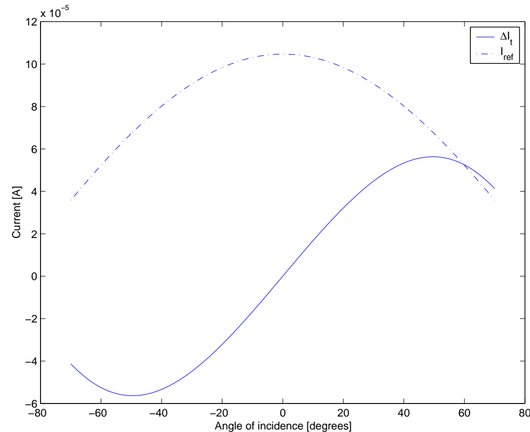

Figure 7: Ideal ΔI_t and I_{ref} currents for the chosen geometry.

4 SENSOR REALISATION

The silicon part of the sensor is the most process heavy and requires 59 processing steps involving 5 masks. The Pyrex part is fabricated through 24 steps using 2 masks. However, the two parts can be processed in parallel, reducing the overall production time.

4.1 SOI Wafer

The first main step, and the most critical for resulting efficiency, is the creation of the pn-junctions. This is done by ion implanting B into specific areas of the n-type (P) device layer of SOI substrate;

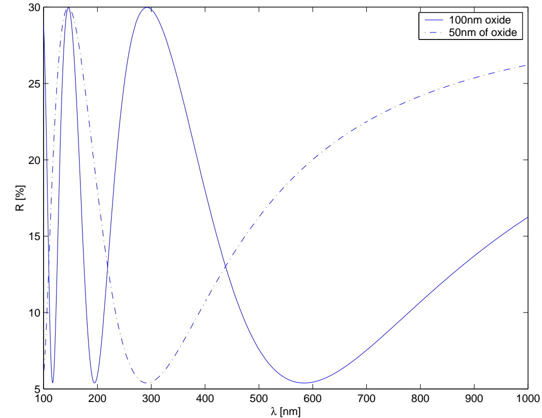

Figure 8: Reflection vs. wave length.

this implant is carried out at a moderate energy to ensure most efficiency at short wave lengths. The ohmic n-type contact is improved by further implant of a high dose of P.

Two concentration levels of B is implanted to optimise the efficiency of the photodiodes. A high dose B is ion implanted with a very low energy to ensure that a higher concentration resides in the upper part of the p well below the contacts. This enables good ohmic contact without a dramatic reduction of the carrier lifetime.

An oxide layer is grown as passivation layer and to act as an optic filter. On the first batch of produced flight sensors the oxide thickness is 1000Å – however as seen on figure 8 a thickness of 500Å would be more appropriate. This step also anneals the implanted ions into the lattice. Subsequently contact holes are etched in the oxide followed by evaporation of contact metals. Finally electrical separation of the different pn junctions is obtained by a combination of wet and dry etch. This final fabrication step and the subsequent cleaning procedures of the SOI wafer is especially crucial. An uncontaminated and well structured interface is required for successful anodic bonding without voids and discharges over electrically sensitive areas. The latter hazard is minimised by proper control of the increase in bonding voltage.

4.2 Pyrex Wafer

Creating the slit structure on the Pyrex wafer is straight forward using e-beam evaporation. The most critical and time consuming part is the structuring of the cavities, which are to encompass the structures on the SOI wafer. A Cr layer is deposited prior to creating the slit on the opposite side. This

enables a better subsequent etching of the cavities without creating pinholes in the anodic bonding interface. Low contamination levels are ensured by extensive cleaning of the surfaces using active oxygen and Piranha clean (H_2SO_4/H_2O_2). Cr is used as an adhesive layer for the Au defining the slit, but is not affected by the oxygen plasma due to the protection offered by the Au during the relative short exposure to active oxygen.

4.3 Dicing

After successful anodic bonding the wafer is diced. Figure 9 shows how the wafer stack is diced. Three lines are cut in the bonded wafer pair: Lines no. 1 and 2 are 400μm deep and line no. 3 dices the chips.

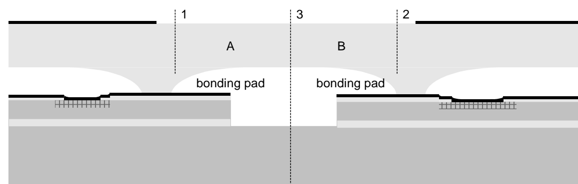

Figure 9: Dicing method.

A and B in figure 9 are manually removed after dicing. The sensor is wire bonded using Al wire, once the chip is mounted on the PCB.

4.4 Process Sequence

An overview of the used process sequence is given below.

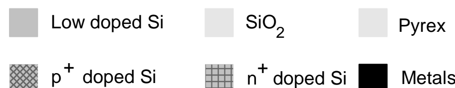

500μm SOI substrate, p-type device layer. A thin thermal oxide is grown followed by a three step implantation process – along with needed wet etches through the oxide – that creates the pn junction and ohmic contacts to the p-layer.

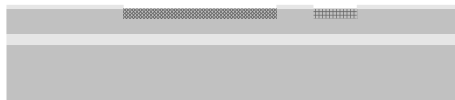

Contact holes are wet etched. Ti/Al contacts from the pn junctions to the wire bonding pads are evaporated using e-beam. Ti is employed to prevent diffusion of Al into the silicon.

The devices are electrically insulated by wet etching through the two oxide layers and anisotropic Reactive Ion Etching (RIE) through the intervening silicon layer.

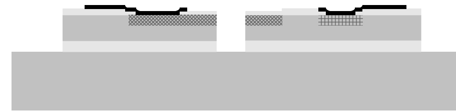

A 1000Å Cr layer is deposited on the 500μm Pyrex wafer as an additional masking material against later HF etching. Next the optical slit is created on the other side and is defined by a 2000Å Au layer using 150Å Cr as adhesive.

Cavities are etched by first removing Cr to create etch holes followed by the isotropic HF etch. Finally the remaining Cr is removed leaving a pure Pyrex bonding interface. During this process the slit side of the wafer is protected by high etchant resistent tape.

Finally the two wafers are anodically bonded at a temperature of 350°C at 700V. A Si wafer with 160Å oxide is placed on top of the Pyrex wafer during bonding to protect the Au defining the slit.

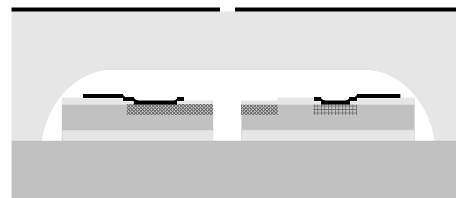

5 INTEGRATION

On DTUsat the sun sensor is integrated with the mechanical structure as illustrated in figure 10 and 2. The sensor chip is glued directly to the PCB containing the necessary measurement and interface electronics. Electrical contact between the chip and the gold-plated PCB is realised with direct wire bonding. To protect the wire bonds – especially during assembly of the satellite – the chip is surrounded with a palisade consisting of 8 pieces of component

wire soldered to the PCB in the interior; the palisade was chosen since this solution was less time consuming than finding an encapsulation that also protects the wire bonds during thermal cycling. A more reliable solution is mentioned in section 8.

The dimensions of the PCB is $3.9 \times 5\text{mm}^3$ and it has a mass of 7.1g including sensor chip, kapton tape, palisade, and nuts. Estimates yield that this can be lowered to below 3g if two layer PCBs and further component packing is employed; however this will increase the experienced noise.

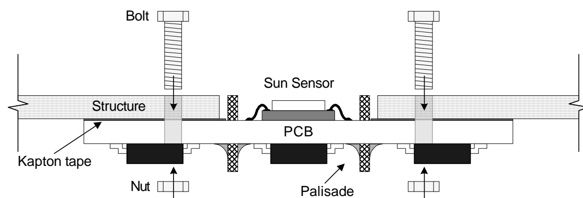

Figure 10: Sketch of the mechanical integration of the sun sensor on DTUsat.

The division described in section 2 is carried out by using a true bipolar and fully differential analog input ADC (AD7450B). The difference and reference signals are amplified and feeded to the input and reference pins respectively. This method has the advantage that the number of needed components are very low (8 ICs including interface logic and a temperature sensor behind the sensor chip in the interior) and that effects from drift on e.g. reference signals during amplification are removed. Of course the method sets limitations on the obtainable resolution for low supply voltages; with the current implementation 10bit is obtainable.

5.1 Calibration

Requirements from the payload to attitude determination are quite low; the accuracy obtained by investigating the mechanical assembly is simply enough. Therefore no calibration was performed to establish relations between sensors and the body frame.

However, to enable in space validation of DTUsat's sun sensors and magnetometer[4] precise co-calibration is desired. This calibration was accomplished with a variety of the method proposed by Merayo *et. al.*[5] By doing half-sphere measurements on a known constant magnetic field and a known solar position with the magnetometer and each sun sensor respectively the desired sun sensor-magnetometer relations can be determined to great accuracy.

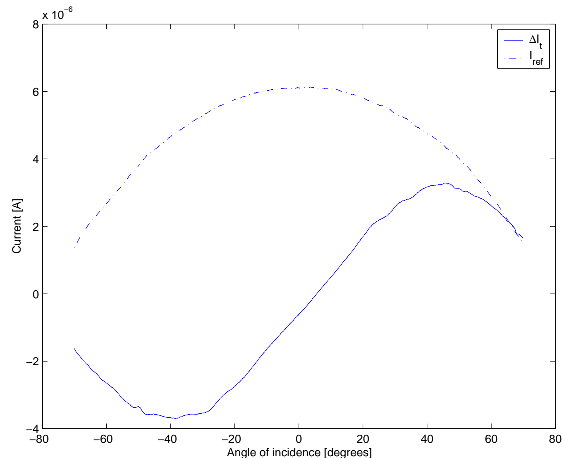

Figure 11: Measured ΔI_t and I_{ref} currents from a sensor chip.

6 PERFORMANCE

Figure 11 shows measured ΔI_t and I_{ref} from a sensor chip. The amplitudes on these graphs are of course much lower than what is expected in space. The reason for this is the low power density from the used collimated Xenon lamp. Calculations along with experiments have confirmed that the amplitude will be around the desired 100μA at 0°. With this amplitude correction the obtained results are close the ones of the ideal device shown in figure 7. The efficiency of the second batch, which still is to be manufactured, is expected to be higher with the improvements in the optical filter suggested in section 4 – which might mean that the sensor easily can be scaled further down.

In figure 12 $\Delta I_t/I_{ref}$ has been calculated from the data in figure 11. This is not as linear as the ideal device which of course is due to imperfections in figure 11. At large angles the output is not single valued in some small regions which of course limits the obtainable resolution in these regions. This is due to the bumps seen in figure 11; investigations on these are to be conducted and hopefully removed in the second generation. An offset error is also present due to an offset in ΔI_t, which is due to difference in efficiency for the two triangles. The device is of course still useable with these imperfections since interpolation or a look-up table can be used instead of some linear parameters.

The standard deviations for the characteristics in figure 11 and 12 is plotted in figure 13 along with the output of an ADC (similar to the graph in figure 12) of a pre-flight unit. The deviation of zero above

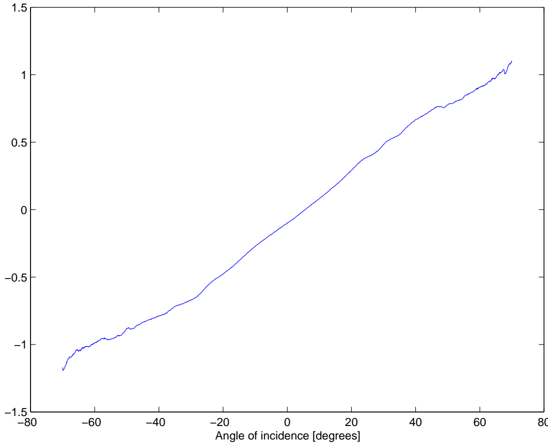

Figure 12: Calculated response from an ideal division.

$\sim -65°$ is due to saturation during the experiment, and the peaks are due to start-up problems in the test setup. The flight units naturally do not posses these imperfections.

In the region $-50°$ to $50°$ the standard deviation is within 5 engineering units, which with the used 12bit ADC corresponds to errors $\leq 0.17°$.

Due to to the short available testing period on DTUsat it has not yet been tested what performance that can actually be achieved in space. However, from the above example and the graphs it is clear that systems with a resolution of at least 1° should be feasible in the $-40°$ to $40°$ region. For larger angles it might be difficult to achieve a resolution below 1° due to increased noise (due to decreasing I_{Iref}) and the bumps in figure 12.

7 NEED FOR SPACE-MEMS

Acronyms are prevalent in both the space and MEMS society[§], and today it *almost* seems like this is the only thing the two societies have in common. However, the authors find Space-MEMS more interesting for both societies than just being another acronym, SMEMS, which is a bit more peculiar than most acronyms since it is also a palindrome.

Of course the above description is pushing it to the extremes since MEMS is being applied more and more – the pace is just too slow, and why is that? Below is some of the "allegations" the authors have met.

[§]In this text "MEMS society" includes all fields from both the micro and nano world.

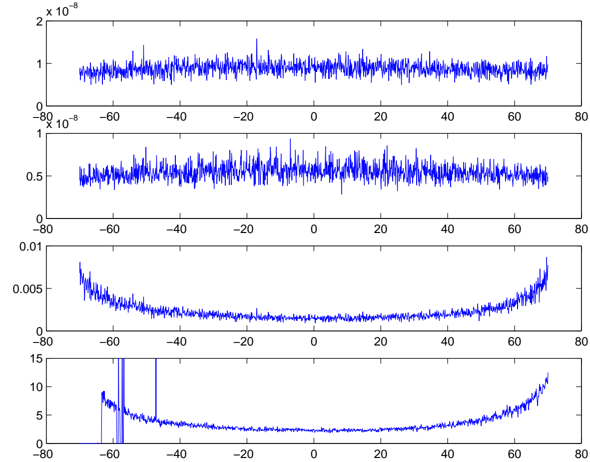

Figure 13: Standard deviations for ΔI_t, I_{ref}, $\Delta I_t/I_{ref}$ and $\Delta T_t/I_{ref}\big|_{ADC}$ for an early validation test of the pre-flight electronics and sensor. The units are A for the first two, the third is dimensionless, and the fourth is in engineering units of the ADC.

Lack of robustness! Is often an argument, which does not hold. The small dimensions actually make the devices more robust while it is possible to mass produce completely identical systems. This and the small size and mass makes redundance much easier while having more robust systems!

Too expensive! Perhaps. Realising an all MEMS spacecraft is of course very time consuming and expensive. However, many components that do exist today can easily and quite cheap be "translated" directly into MEMS equivalents; one example is the presented sun sensor. Doing this has the advantage that the components are more easily produced in the future and that one gain the advantages that MEMS possesses. Other components are simply not possible without MEMS.

Another reason to why MEMS often seem to expensive is that the trend for SMEMS today is that most companies/departments etc. that need MEMS start doing MEMS themselves instead of utilising the already well-established MEMS society. This seems quite surprising.

Our systems won't shrink! Is an argument often given because they still need e.g. large connectors for interfacing which then results in very little mass and volume reduction when

MEMS is employed. This seems like a rather bad excuse for not being creative. Of course smaller and smarter interfaces are wanted now as well as in the future. The ones we are using now can in many cases be dated back to the creative Apollo days. How come wireless (e.g. optical or radio) interfaces are not the standard today? These simplifies the harness and structure of a spacecraft to great extent since it becomes very modular.

What can be done? From the above examples it seems like informing space professionals about MEMS and trying to help establishment of collaborations would be a great help. Special initiatives towards many space companies are also needed since they do not have or cannot afford facilities for doing MEMS, which obviously results in counteractions towards MEMS.

Information from e.g. space agencies to universities and companies involved with MEMS is also insufficient today. More information ought to be channeled directly to all important laboratories and not just to space laboratories; such as e.g. letters on workshops, congresses, and contracts that might be of their interest. Non-space laboratories will not come across many space activities if they do not take initiatives themselves. To help others interested in SMEMS the authors have come across ESA's Annual Round Table on Micro/Nano Technology and CANEUS, which is a biennial aerospace MEMS conference; the second conference is in Monterey, CA 2004.

Some in the space society, the group the authors regard as the "conservative", say that the MEMS society might as well could be the ones to initiate the collaborations. This is nonsense since the MEMS society has enough applications today to test their principles in e.g. medico science – the gain for them is quite low. However, the space society can only gain since MEMS enables all kinds of new experiments in space. One example could for instance be taken from the medico area: In Micro Total Analysis Systems (μTAS) liquids can for instance be analysed on a chip which make these devices ideal for various probing missions.

A very good initiative from the space agencies would be to offer R&D projects to universities which does not necessarily have to end up in a final flight device. In this way the universities can help doing all the research – and they might select the space applications in favour of other applications since "space" is a magic word – and the space professionals can use the results to develop flight devices in cooperation with the universities. Perhaps the previously mentioned interface problem could be solved quite fast to make integration of SMEMS easier?

We do know that these easy words do not remove the current gap between the two societies, but the hope is that it can help setting more focus on the problem. "Just" being M.Sc. students trapped in the cross field seing all this potential not being utilised is quite frustrating.[¶]

8 FUTURE WORK

Naturally further investigations and improvements of the sun sensor are to be conducted. One additional feature could be to create anti-reflective coatings under the Cr/Au slit and on the Pyrex surface in the cavity to avoid reflections of reflected light in the Pyrex-cavity transition and from the sensor area which is often a problem in traditional devices; how serious this problem is for the designed sensor is to be investigated.

As stated in section 5 a better method for making electrical connections is desired. One way of doing this is to employ so called interconnects which routes contact to the backside of the SOI wafer. With this method the chip can be soldered directly to a substrate or PCB without the need of fragile wire bonds. Interconnects has e.g. been studied by Heschel.[3]

Since it seems like no post-flight data will become available from DTUsat the authors are of course interested in missions that will fly a prototype for space validation. This could also help lifting the project from the student level where it currently resides.

As mentioned in the description of DTUsat a MEMS electron emitter has also been developed at MIC.[1] This device was however not finished in time so work on this device is also continued.

A new Space-MEMS project that has been started at MIC is an electric propulsion system based on ion-propulsion.

[¶]Opinions stated in this section is opinions of the corresponding author and may not correspond to MIC's opinion.

9 CONCLUSION

A two-axis MOEMS sun sensor measuring $\sim 7 \times 8\text{mm}^2$ with $\pm\text{FOV} = 70°$ has been designed, tested, and flown on DTUsat. Resolution better than 1° is obtainable in the region −40° to 40° and beyond these angles a resolution below 1° is considered difficult. The first generation of the sensor is not linear enough to be used as a linear sensor – interpolation or look-up tables is needed.

One complete sensor chip along with needed measurement and interface electronics was implemented on a $3.9 \times 5\text{cm}^2$ PCB with a mass of 7.1g; estimates have shown that the mass can be reduced to at least 3g.

In the paper a small discussion on *Space-MEMS* is given.

ACKNOWLEDGEMENTS

The work carried out on the MOEMS Sun Sensor is a continuation of ideas proposed in collaboration with M.Sc. student K. Krogsgaard[2] – whom finalised the proposed magnetometer[4]. M.Sc. students M. Pedersen and J.H. Hales wishes to thank their advisor Process Specialist M.Sc. R.W. Fléron for his great enthusiasm and guidance. Lastly the DTUsat group is thanked for the joint effort.

Development and manufacturing costs are mainly being sponsored by Mikroelektronik Centret (MIC). The DTUsat project is partially funded by the Public Space Research Committee through the Ministry of Science, Technology and Innovation. Several other foundations and companies have also contributed to various task groups within DTUsat.

ESA's European Student Outreach Programme is sponsoring participation of M. Pedersen and J.H. Hales at the 54$^{\text{th}}$ IAC.

REFERENCES

1. R.W. Fléron, M. Pedersen, J.H. Hales, P.R. Bidstrup, and A. Torp. *Two-Axis MOEMS Sun Sensor and MEMS Electron Emitter developed at MIC for DTUsat.* ESA 4th Round Table on Micro/Nano Technologies for Space, 2003.
2. J.H. Hales, M. Pedersen, and K. Krogsgaard. *Attitude Control and Determination System for DTUsat.* B.Sc. project at Department of Automation, Ørsted•DTU and Mikroelektronik Centret (MIC) at The Technical University of Denmark, 2002.
3. Matthias Heschel. *Multiple Through-Wafer Interconnects for Stacking of Microelectromechanical Devices.* PhD thesis, Mikroelektronik Centret (MIC) at The Technical University of Denmark, 1999.
4. K. Krogsgaard. *Compact Vector Magnetometer for Pico Satellites.* 17th Annual AIAA/USU Conference on Small Satellites, 2003.
5. J.M.G. Merayo, P. Brauer, F. Primdahl, J.R. Petersen, and O.V. Nielsen. *Scalar Calibration of Vector Magnetometers.* Department of Automation, Ørsted•DTU at The Technical University of Denmark, 1999. Published in Meas. Sci. Technol. 11 (2000).
6. Robert Twiggs and Jordi Puig-Suari. *CUBESAT Design Specifications Document.* 2001. http://ssdl.stanford.edu/cubesat/specs-1_files/CubeSat Developer Specifications.pdf.
7. Steen Weichel. *Silicon to Silicon Wafer Bonding for Microsystem Packaging and Formation.* PhD thesis, Mikroelektronik Centret (MIC) at The Technical University of Denmark, 2000.